EUROPEAN ORGANIZATION FOR NUCLEAR RESEARCH

CERN-EP/89-113
4 September 1989

INCLUSIVE PHOTON PRODUCTION IN pA AND AA COLLISIONS AT 200 GeV/u

HELIOS COLLABORATION

T. Åkesson[3], S. Almehed[3], A.L.S. Angelis[19], N. Armenise[1], H. Atherton[3], P. Aubry[8], H.W. Bartels[4], G. Beaudoin[8], J.M. Beaulieu[8], H. Beker[3], O. Benary[18], D. Bettoni[3,a], V. Bisi[19], I. Blevis[21], H. Bøggild[3,b], W. Cleland[12], M. Clemen[12], B. Collick[12], F. Corriveau[7], S. Dagan[18], K. Dederichs[3,c], S. Dell'Uomo[13], P. Depommier[8], R.C.E. Devenish[3,d], S. Di Liberto[13], N. DiGiacomo[5], J.R. Dodd[20], B. Dogolshein[10], A. Drees[4], H. En'yo[3], B. Erlandsson[17], M.J. Esten[20], C.W. Fabjan[3], P. Fischer[4], Z. Fraenkel[21], A. Gaidot[15], F. Gibrat-Debu[15], P. Giubellino[19], P. Glässel[4], U. Goerlach[4], R. Haglund[6], L.A. Hamel[7], H. van Hecke[5], V. Hedberg[3], R. Heifetz[18], A. Hölscher[4], B. Jacak[5], G. Jarlskog[6], S. Johansson[6], H. Kraner[2], V. Kroh[4], F. Lamarche[7], C. Leroy[7], D. Lissauer[2,18], G. London[15], B. Lörstad[6], A. Lounis[8], F. Martelli[19,22], A. Marzari-Chiesa[19], M. Masera[19], M.A. Mazzoni[3], E. Mazzucato[7], M.L. McCubbin[19], N.A. McCubbin[14], P. McGaughey[5], F. Meddi[13], U. Mjörnmark[6], M.T. Muciaccia[1], S. Muraviev[9], M. Murray[12], M. Neubert[4], S. Nilsson[17], L. Olsen[2], Y. Oren[18], J.P. Pansart[15], Y.M. Park[12], A. Pfeiffer[4], F. Piuz[3], V. Polychronakos[2], G. Poulard[3], M. Price[3], D. Rahm[2], L. Ramello[19], L. Riccati[19], G. Romano[16], G. Rosa[13], L. Sandor[3], J. Schukraft[3], M. Sekimoto[3,e], B. Sellden[17], M. Seman[3,f], A. Shmeleva[9], V. Sidorov[11], S. Simone[1], Y. Sirois[7], H. Sletten[3], S. Smirnov[10], J. Soltani[4], W. Sondheim[5], H.J. Specht[4], I. Stumer[2], J. Sunier[5], V. Tcherniatin[10], H.H. Thodberg[3], J. Thompson[12], V. Tikhomirov[9], I. Tserruya[21], G. Vasseur[15], R. Veenhof[3,g], R. Wigmans[3,g], P. Yepes[7]

(Submitted to Z. Physik C)

1) University of Bari and INFN, Bari, Italy
2) Brookhaven National Lab., Upton, NY, USA
3) CERN, Geneva, Switzerland
4) University of Heidelberg, Fed. Rep. Germany
5) Los Alamos Nat. Lab., Los Alamos, NM, USA
6) University of Lund, Sweden
7) McGill University, Montreal, Canada
8) University of Montreal, Canada
9) Lebedev Phys. Inst., Moscow, USSR
10) Phys. Eng. Inst., Moscow, USSR
11) Inst. Nucl. Phys., Novosibirsk, USSR
12) University of Pittsbourgh, Pittsbourgh, USA
13) University of Rome and INFN, Rome, Italy
14) Rutherford Appleton Laboratory, Didcot, UK
15) DPhPE, CEN-Saclay, Gif-sur-Yvette, France
16) University of Salerno and INFN, Salerno, Italy
17) University of Stockholm, Sweden
18) University of Tel Aviv, Israel
19) University of Turin and INFN, Turin, Italy
20) University College, London, UK
21) Weizmann Institute, Rehovot, Israel
22) Angelo Della Riccia fellow

Visitors at CERN from:
a) University of Syracuse, Syracuse, NY, USA
b) Niels Bohr Institute, Copenhagen, Denmark
c) University of Munich, Fed. Rep. Germany
d) University of Oxford, UK
e) Insitute of Nuclear Study, Tokyo, Japan
f) Slovak Academy of Sciences, Kosice, Czechoslovakia
g) NIKHEF-H, Amsterdam, The Netherlands

Abstract

Inclusive photon $p_\perp$ spectra were measured with 200 GeV/u proton, ^{16}O and ^{32}S beams on W and Pt targets, using a conversion method. The measurement of charged pions in the same apparatus allows a comparison of the γ data with the expected γ's from hadronic decays ($\pi^0, \eta, \eta', \omega$). In all data sets, no deviation from the expected shape is observed in the range of $0.1 < p_\perp < 1.5$ GeV/c. The number of photons normalized to pions agrees within the statistical (4% – 11%) and systematical (9%) errors with the number of photons expected from hadronic decays in the integrated ranges of $p_\perp > 0.1$ GeV/c and $p_\perp > 0.6$ GeV/c.

1. Introduction

The study of photon production in heavy ion collisions is motivated by the search for thermal radiation from the system formed in the nucleon-nucleon collisions, e.g. a quark gluon plasma [1]. The data presented in this paper were taken with the HELIOS spectrometer which combines 4π calorimetry with the detection of charged multiplicity, inclusive particle spectra and lepton pairs. Photons are measured via the conversion method in parallel with charged particles in a magnetic spectrometer, spanning an angular range of 15° to 45° in θ_{lab}. Photons provide a unique tool to study hadronic interactions, since they couple directly to the electric charge of the quarks and escape the collision unaffected by final state interactions or fragmentation processes. Direct photons can be emitted both as thermal radiation from the deconfined state [2,3], and as coherent bremsstrahlung signalling the slowing-down of the nuclear proton distribution [4]. The main problem in measuring direct photons is the dominance of hadronic sources. Up to several hundred particles, dominantly pions, are created in these collisions [5]. Since the neutral π^0 decays into two photons, one deals with roughly the same number of decay γ's as charged pions. To get a handle on direct photons, a detailed knowledge of the properties of the produced pions is essential.

In this paper we concentrate on the comparison of the measured photon $p_\perp$ spectra with the expected spectra from hadronic sources which were extracted from charged pion $p_\perp$ spectra measured in the same set-up. Data from proton, oxygen and sulfur beams at 200 GeV/u with W and Pt targets are compared. The number of photons normalized to pions agrees within the statistical (4% - 11%) and systematical (9%) errors with the number of photons expected from hadronic decays.

2. The Experimental Set-up

The magnetic spectrometer of the HELIOS experiment, shown in Fig. 1, views the target through a narrow slit in the calorimeter wall, covering the pseudorapidity interval $1.0 < \eta < 1.9$. The slit of 10 cm height corresponds to a ϕ-acceptance varying from 2.1% at $\eta = 1.9$ to 0.75% at $\eta = 1.0$. The uranium calorimeter above the slit is supported by an aluminum honeycomb ('hexcel'), which amounts to 3% of a radiation length. A magnet with a momentum kick of ~80 MeV/c and two high-resolution drift chambers determine the momentum of charged particles. The z-coordinate is defined as the 15 degree line (see Fig. 1), the x and y-coordinates are defined as horizontal and vertical, respectively. The resolution of the drift chambers which measure the horizontal coordinate via the drift time ($\sigma \simeq 200$ μm) and the vertical coordinate via charge division ($\sigma \simeq 1.0$ cm for p+W, O+W, and 0.3 cm for S+W data), allows elimination of the background from the calorimeters around the slit [6]. In general, the target position

is used for the momentum reconstruction. Below about 1 GeV/c, however, multiple scattering in the material in front of the drift chambers becomes a large effect, and the target point is effectively ignored. The momentum resolution $\delta p/p^2 = 0.08$ for $p \lesssim 1.0$ GeV/c is then limited by the chamber resolution, but reaches $\delta p/p = 0.12$ for $p \gtrsim 1.0$ GeV/c, when the multiple scattering becomes the limiting factor.

An iron converter with a thickness of 5.7% of a radiation length placed directly in front of the first drift chamber allows the measurement of photons in the same apparatus via the observation of the converted electron-positron pair. Two planes of multiwire proportional chambers (COMET) bracketing the converter allow localization of the conversion point. The wires of the proportional chambers are vertical and separated by 2.5 *mm*. For the first 248 wires (closest to the beam), the readout electronic groups two wires into one channel, and for the remaining 496 wires, four wires are grouped together.

3. The Data Sets

Four data sets are presented in this work: p+W, ^{16}O+W, ^{32}S+W and ^{32}S+Pt. Since the ^{32}S+W and ^{32}S+Pt data do not show any difference for photons as well as for pions, both targets are treated together for the ^{32}S beam. For ^{16}O+W (^{32}S+W) data, a 0.1 mm (0.2 mm) disk was used as a passive target. For p+W and ^{32}S+Pt, an active target was used; the potential wires of a drift chamber served as targets. As in [6], we only use the last four wires to reduce multiple interactions to $< 10\%$.

The trigger for these data required a valid interaction, as described in [5], and also used the transverse energy measured in the calorimeters in the pseudorapidity range $-0.1 < \eta < 2.9$. Varying scale-down factors for different E_T thresholds were used for the ion runs, providing similar statistics across the E_T range. The number of reconstructed photons per data set is shown in Table 1.

TABLE 1:

data set	photons	target
p+W	529	active; 1 mm wires
^{16}O+W	297	disk 0.1 mm
^{32}S+W	850	disk 0.2 mm
^{32}S+Pt	105	active; 0.2 mm wires

A local anticoincidence requiring no COMET signal before the converter and a COMET hit after the converter was used as a photon trigger for the p+W data, selecting central

collision events by requiring $E_T > 20$ GeV. This trigger was not used during the ion beam, since the multiplicity was too high to get a resonable selectivity on photons.

4. Data analysis

The aim of the analysis is to find photons originating from the target which travel through the slit, convert in the iron plate between the COMET chambers to e^+e^--pairs, which in turn open in the magnetic field between the drift chambers (see Fig. 1). A detailed description of the whole photon analysis chain is given in [7]. For each event, track reconstruction starts with the 'segments' found separately in DC4/5. A track is defined by a DC4 segment pointing to the same region in the center of the magnet as a DC5 segment; the corresponding segments are used to determine the momentum of the track. A photon candidate is defined as a combination of two tracks with the same DC4 segment. From this it is clear that the mass of the e^+e^--pair is zero by definition.

In the case of active target data, offline analysis determined the wire at which the interaction took place, and rejected interactions outside the target. The performance of the active target and the algorithm to find a wire is described in [6]. The origin from the target was secured by 'standard' target cuts in vertical and horizontal directions (for details see ref. [6]). As discussed in section 6, the systematic error due to the cuts is minimized by cutting on just one of the electron tracks, selected randomly.

The next step of the photon analysis positively identifies the conversion in the iron plate between the two COMET chambers, essential for the absolute normalization. For a photon candidate in the drift chambers DC4/5, a local COMET veto is required, i.e., no hit in the first plane corresponding to the two tracks. The efficiency of the veto plane is determined by charged particles requiring a match of the reconstructed track in DC4/5 with a COMET hit within ± 1.5 *cm* horizontally. It was found to be 93%, 85% and 90% for p+W,O+W and S+W(Pt), respectively. It should be mentioned that for the p+W data a local match of DC4/5 tracks and the second COMET plane is required ($\varepsilon = 60\%$), since a COMET γ-pattern (locally a hit in the second plane without a hit in the first plane) was used to trigger on photons. The efficiency of this trigger was determined offline and found to be 95%.

The background in the photon sample is measured by the number of like-sign pairs; the ratios of like to unlike-sign pairs are 2%,12%,16% and 32% for p-W,O-W,S-W and S-Pt respectively. These are due to random tracks formed from DC4 and DC5 segments, which do not belong to the same particle. The amount of random tracks is measured by mixing DC4 and DC5 segments from different events of comparable transverse energy ($\simeq$ charged multiplicity). The ratio of random tracks in the S+W data sample is 23% before the 'standard' cuts and 3% afterwards, normalized to the number of tracks in

the unmixed sample. The main contributions to the background in the photon sample are:

i) charged hadrons without a hit in the COMET veto plane (inefficiency) whose DC4 segment forms an additional, random track with another DC5 segment.

ii) a real e^+e^--pair, where one low-momentum electron curls up in the magnetic field, does not reach DC5 and is replaced by a random track.

A quality test can be done with the relative energy distribution of the e^+e^--pair

$$\epsilon \equiv \frac{E_{e^\pm}}{E_{e^+} + E_{e^-}}$$

The results are shown in Fig. 2 for an ideal detector, S-W data, Monte Carlo and background photons. The background tends to have a more asymmetric ϵ distribution. Therefore the following cut was applied:

$$\epsilon_{cut} < \epsilon < 1 - \epsilon_{cut}$$

ϵ_{cut} was chosen to be 0.0, 0.2 and 0.1 for p+W, O+W and S+W(Pt) data, respectively, as a compromise between statistics and background. After this cut, the remaining background (like-sign pairs) was found to be 2%, 12% and 16% for p+W, O+W and S+W(Pt), respectively, and was subtracted from the data.

The measured $p_\perp$ spectra have to be corrected for various detector effects, e.g. geometrical acceptance, finite momentum resolution and multiple scattering, which influence the shape of the spectra. Therefore, photon $p_\perp$ spectra were simulated including all detector properties, using a Monte Carlo programme with the generator described below, and reconstructed using the full analysis chain. The ratio of input spectra to the results from the simulation is used to correct the measured data. The photon generator is designed to describe photons from hadronic decays. The relevant hadrons and their contributions (normalized to π^0) are taken from ISR pp data: η (14.5%), η' (6.3%), ω (11%) [8]; all numbers are integrals over the whole range of $p_\perp$ using m_T scaling. The $p_\perp$ distribution of the π^o was assumed to be the same as for $\pi^\pm$ and was derived from π^- data measured in the same instrument for the respective reaction [6]. For the other mesons, the $p_\perp$ spectra were derived from the π^0 spectrum assuming scaling with the transverse mass [9] $m_\perp = \sqrt{m^2 + p_\perp^2}$ as

$$f(p_\perp; h) \sim f(p_\perp; \pi^0) \cdot \left(\frac{m_\perp(p_\perp; \pi^0) + 2.0 \text{ GeV/c}^2}{m_\perp(p_\perp; h) + 2.0 \text{ GeV/c}^2} \right)^{12.3} \quad ; \quad h = \eta, \eta', \omega$$

The rapidity distribution of the hadrons was taken from the calorimeter $dE_T/d\eta$ data [10].

5. Normalization of the data

To search for possible sources of direct photons, the measured data must be compared with the background from hadronic decays. Therefore, we investigated the ratio

$$r_\gamma = \frac{N^\gamma}{N^{\pi^\circ}} = \frac{\int \frac{\mathrm{d}N^\gamma}{\mathrm{d}y\mathrm{d}p_\perp}\mathrm{d}y\mathrm{d}p_\perp}{\int \frac{\mathrm{d}N^{\pi^\circ}}{\mathrm{d}y\mathrm{d}p_\perp}\mathrm{d}y\mathrm{d}p_\perp} \equiv \frac{\gamma_{all}}{\pi^0}$$

If one would just deal with π^0's and integrate over the whole range of $p_\perp$ and y, r_γ would be equal to 2. The HELIOS external spectrometer measures γ's with $p_\perp > 100$ MeV/c over a restricted range of y (see above). Integrating over this acceptance and including all additional hadronic γ sources (η, η', ω), one would expect $r_\gamma \simeq 1.6$ for the S+W data. A detailed discussion of the expected values of r_γ for the data sets investigated follows below.

In a given data set, the number of π^0's is identified with the number of negative tracks (π^-'s) measured in the external spectrometer. The contamination by conversion electrons is $\simeq 4\%$ for $p_\perp > 100$ MeV/c. This number is derived using Monte Carlo simulations on comparable numbers of π^- and $\pi^0, \eta, \eta', \omega$. It was checked to give correct results in the low-momentum region, where the time-of-flight system of the external spectrometer allows separation of electrons and pions. The K^- contamination in the raw sample of negative tracks is also measured by the time-of-flight system. It is 2% for $p_\perp > 100$ MeV/c and reaches 8% for $p_\perp > 600$ MeV/c [11]. The relevant numbers for K^-'s are those which did not decay before entering the detector, and thus must not be corrected for decays and different acceptances in rapidity for π^- and K^-. Antiprotons are not visible in our data, i.e., $\bar{p}/\pi^-$ is certainly below 1% [11]. The fraction of random charged tracks is determined by mixing events (see above) and amounts to 1%, 3% and 3% for p+W, O+W and S+W data, respectively. The Monte Carlo programme was used to correct for the remaining detector effects like decays, geometrical acceptance, hardware and software efficiencies.

To get the number of photons in a given data set, one has to consider the 5.7% radiation length of the 1 mm iron plate. The air between target and COMET chambers and the hexcel in the slit amounts to 4% of a radiation length. This leads to two effects in the normalization, which partially cancel each other. First, the photons coming from the target are reduced by $7/9 \cdot 4\%$ because of conversions. Second, these conversions in front of COMET can be misidentified as photons converted in the COMET iron plate due to the inefficiency of the veto plane.

Random hits or pile-up in the first COMET plane could destroy the veto needed for photon identification. This loss was determined quantitatively by mixing COMET

data of different events with comparable transverse energy. About 7%, 13% and 17% of the photons were vetoed for p+W, O+W and S+W, respectively.

The remaining detector effects, mainly the losses of low-momentum electrons in the magnetic field, were corrected by the Monte Carlo programme.

6. Systematic errors

A list of all systematic errors can be found in Table 2. Sources of uncertainties are the following quantities entering linearly into the calculation of r_γ :

- The number of COMET hits as a function of E_T was determined taking the pile-up probability into account. Therefore the ratio of segments found to corrected number of COMET hits serves as a relative measure of the *segment finding efficiency* as a function of E_T. Slightly lower efficiency is observed for the O+W and S+W data. For the p+W data, no effect is seen. The absolute value of the segment finding efficiency is fixed by visual scans of several hundred event displays searching for isolated segment candidates (defined as $E_T = 0$), and counting the number of candidates found by software. The error on the segment efficiency determined this way was estimated to be 5% by comparing the results of different scans. Since a photon or e^+e^- pair needs three segments and a pion just two, this uncertainty enters linearly into r_γ.

- The electron tracks used for the photon analysis have a significantly lower $\langle p_\perp \rangle$ than the tracks of the pion sample. It is therefore important to look for $p_\perp$ - dependent effects. The *segment finding efficiency* is $p_\perp$ -dependent due to the fact that low-momentum particles are deflected more and therefore have a steeper slope in DC5. This leads to a higher probability for these segments to cross drift cell boundaries. At the edges of drift cells, the spatial resolution gets worse, an effect which is taken into account in the Monte Carlo programme. As a result, there is indeed no difference seen in the fraction of cell crossing segments in Monte Carlo and data for different bins of $p_\perp$.

- Events with only one DC4 and one DC5 segment were investigated to test the $p_\perp$ -dependence of the *track finding efficiency*. In those events it was assumed that both segments belong to the same particle, if two additional constraints were fulfilled: (i) the y-information of DC4/5 which is not used in the track fit, was fitted linearly. Requiring the fit to point to the target in the y-coordinate removes random combinations very efficiently. (ii) The two segments were pointed in the x-z plane (top view) to the middle of the magnetic field, where a match within a window of 15 cm is required (standard: 3 cm). Random combinations which pass these requirements were measured using event mixing and found to be negligible.

The same procedure was applied to the Monte Carlo data. For $p_\perp$ -values down to 200 MeV/c, only small differences (3%) are seen, but a significant difference of 8% for $100 < p_\perp < 200$ MeV/c and 24% for the lowest transverse momentum in the bin $50 < p_\perp < 100$ MeV/c is observed. The explanation for this discrepancy between Monte Carlo and data can be found in the lack of knowledge of the x-t relation ($\simeq 1\%$) and additional hits around the real track which may cause some fraction of wrong hit assignments in the segment finding. Both imperfections in the data lead to changes in the slope of the segments and thus to a rather high chance for strongly bent tracks to give a mismatch of the DC4 and DC5 segments. The data were corrected for this effect. The uncertainty in the magnitude of this low-$p_\perp$ correction leads to a systematic error in r_γ of 5% for $p_\perp > 100$ MeV/c and 2% for $p_\perp > 600$ MeV/c.

- To accept a photon or pion, certain *cuts* on the quality of the electron/positron or pion tracks have been applied. r_γ is proportional to the ratio of measured γ's to π^-'s. To be independent of the cut efficiencies, the cut in the photon sample was applied on just one of the observed two tracks. The slightly increased background is determined by the number of like-sign pairs and is subtracted. To study the stability of r_γ, the quality cuts were varied by a factor of 2 and demonstrate a stability of r_γ within 3 %.
- The track finding routine does not allow two tracks to share the same DC5 segment. If this happens, only the track with the better χ^2 of the track fit is kept for further analysis. Therefore, the e^+e^- *pair pattern* in the drift chamber consisting of two tracks with the same DC4 segments could be lost by a random track with a different DC4 segment and one of the DC5 segments of the e^+e^- pair. This effect is measured as a function of $p_\perp$ and E_T. The number of random tracks as a function of $p_\perp$ is multiplied with the probability for the random track to have a smaller χ^2 than the tracks in the photon sample. For the S+W(Pt) data, the probability of a random track erasing a photon track is decreasing linearly from 4% for $p_\perp = 100$ MeV/c tracks to 1% for $p_\perp = 1$ GeV/c tracks; for the lowest bin, $50 < p_\perp < 100$ MeV/c, one gets 8%. The uncertainty on this number leads to a systematic error of 2% in r_γ.
- The limited knowledge of the fraction of photons converted in the material before COMET, but counted as COMET photons due to inefficiency of the COMET veto plane leads to a systematic uncertainty of 2% in r_γ. COMET pile up in the veto plane leads to losses in the photon sample (see last section) resulting in a systematic error of 2%.
- The tolerance of the thickness of the 1 mm *iron plate* used as the converter between the COMET chambers is 2%.

- The uncertainty of contamination of the negative track sample with electrons and kaons leads to a systematic uncertainty of 2% on r_γ for $p_\perp > 100$ MeV/c and 4% for $p_\perp > 600$ MeV/c, due to the larger kaon fraction for high $p_\perp$.

Adding all contributions quadratically one gets an overall systematic error of 9% on r_γ for $p_\perp > 100$ MeV/c, and 8% on r_γ for $p_\perp > 600$ MeV/c.

The experimental value of r_γ has to be compared with the expected value r_{γ,h^o} from hadronic sources:

$$r_{\gamma,h^o} \equiv \frac{\gamma_{hadronic}}{\pi^0}$$

Table 2: Systematic errors on r_γ ($p_\perp > 100$ MeV/c)

calculation of r_γ from experimental data	segment finding	±5%
	$p_\perp$ -dependent tracking efficiency	±5%
	analysis cuts	±3%
	random tracks	±2%
	conversions before COMET	±2%
	COMET pile up	±2%
	COMET iron plate thickness	±2%
	e^-, K^- fraction in π^- sample	±2%
	quadratic sum :	±9%
calculation of r_{γ,h^o} from hadronic decays	η/π at 2.5 GeV/c	$^{+7.5}_{-3.5}$%
	m_T scaling	$^{+0.0}_{-7.5}$%
	difference of π^- and π^0 spectra	±1.5%
	rapidity distribution of $(\pi, \eta, \eta', \omega)$	±1.2%
	quadratic sum :	$^{+7.7}_{-8.5}$%

The photon generator described in section 5 was used to determine r_{γ,h^o}. Four sources of uncertainties in the calculation of this number are discussed:

- The ratios η/π^0, η'/π^0 and ω/π^0 were taken from ISR measurements of pp reactions with comparable $\sqrt{s}$. For heavy ion collisions, no values are published so far on these ratios. Preliminary results of the WA80 collaboration [12] are 40% higher than the ISR values in the range $2.0 < p_\perp < 2.4$ GeV/c, but still agree within the error bars with the ISR value. Therefore, the η/π^0 (η'/π^0 ,ω/π^0) fraction was varied between +40% and −20% to describe reasonable uncertainties of heavy meson production. This leads to an uncertainty of +7.5% and −3.5% in r_{γ,h^o}.
- The η/π^0 (η'/π^0 ,ω/π^0) fraction as a function of $p_\perp$ is generally described by m_T scaling. A recent paper (last ref. in [8]) has investigated the low-$p_\perp$ behaviour

of η/π^-. The shape of m_T scaling was changed in a way to be still in reasonable agreement with these data. This leads to an uncertainty of +0% and −7.5% in r_{γ,h^o}.

- The π^- $p_\perp$ spectrum was assumed to be the same as the π^0 $p_\perp$ spectrum. The difference of π^+ and π^- $p_\perp$ spectra was measured in ISR pp collisions [13]; it corresponds to a 1.5% difference in r_{γ,h^o}.
- The rapidity distributions of the hadrons were assumed to be the same as the measured HELIOS $dE_T/d\eta$ distribution. In the range of $0 < y < 3$, this hypothesis was changed assuming a distribution which increases by a factor of three faster than the measured data. This extreme assumption would lead to a 1.2% change in r_{γ,h^o} measured in $1.0 < \eta < 1.9$.

Altogether one gets an uncertainty on r_{γ,h^o} of +7.7% and −8.5% for $p_\perp > 100$ MeV/c. Equivalent investigations were made in the range $p_\perp > 600$ MeV/c, leading to uncertainties on r_{γ,h^o} of +9.4% and −8.3%.

7. Results

Figs. 3 a,b,c show the corrected inclusive $p_\perp$ spectra for photons observed in p+W, ^{16}O+W and ^{32}S+W(Pt) at 200 GeV/u, respectively. These data are taken in the rapidity range $1.0 < y < 1.9$ and the $p_\perp$ range $0.1 < p_\perp < 1.5$ GeV/c. The full line describes the spectra expected from hadronic sources $\pi^0, \eta, \eta', \omega$. The agreement in shape is remarkable. The π^0 photons serve as normalization; the quantity shown in Fig. 3 a,b,c is:

$$\frac{1}{N^{\pi^o}} \left.\frac{dN^\gamma}{dp_\perp}\right|_{1.0<y<1.9}$$

The ratios of ^{16}O to proton data and ^{32}S to ^{16}O data are plotted in Fig. 4a,b, respectively; the normalization is done by the number of photons in each sample. The figures indicate that there are no significant differences in the photon $p_\perp$ spectra when going from p–A to ^{16}O–A to ^{32}S–A collisions at 200 GeV/u.

In Table 3, the values for $r_\gamma = \gamma_{all}/\pi^0$ are listed for all data sets and regions of $p_\perp$ and E_T.

r_γ is determined for all data sets integrated over the region $p_\perp > 100$ MeV/c. Within the statistical and systematic errors, no excess above the hadronic sources is seen. To study a possible rise of γ_{direct}/π^0 with $p_\perp$, as observed in pp collisions, r_γ was evaluated in the integrated region $p_\perp > 600$ MeV/c for the S+W(Pt) sample (case of best statistics). The resulting value again agrees with the expected one within the errors.

Table 3: All values for r_γ are determined integrating over the $p_\perp$ region listed. $\langle E_T \rangle$ is measured in the range $-0.1 < \eta < 2.9$. r_{γ,h^0} represents the photons expected from hadronic sources; here only systematic errors are quoted.

data set	$p_\perp$ range	$< E_T >$	r_γ	r_{γ,h^0}
p+W	$> 100\ MeV/c$	> 20 GeV	$1.56 \pm 0.07 \pm 0.13$	1.54 ± 0.12
O+W	$> 100\ MeV/c$	109 GeV	$1.63 \pm 0.15 \pm 0.15$	1.60 ± 0.13
O+W	$> 100\ MeV/c$	148 GeV	$1.64 \pm 0.15 \pm 0.15$	1.60 ± 0.13
S+W(Pt)	$> 100\ MeV/c$	145 GeV	$1.43 \pm 0.08 \pm 0.13$	1.60 ± 0.13
S+W(Pt)	$> 100\ MeV/c$	200 GeV	$1.51 \pm 0.09 \pm 0.14$	1.60 ± 0.13
S+W(Pt)	$> 100\ MeV/c$	240 GeV	$1.70 \pm 0.14 \pm 0.15$	1.60 ± 0.13
S+W(Pt)	$> 600\ MeV/c$	200 GeV	$0.62 \pm .067 \pm .050$	$0.69 \pm .062$

Recently, thermal radiation originating from interactions between quarks and gluons in a thermalized state was calculated in great detail assuming a phase transition to a quark gluon plasma [3]. From these calculations one would expect a rate γ_{direct}/π^0 of a few percent ($\simeq$ 5% at $p_\perp \simeq 1$ GeV/c). Incidentally, the slope of the thermal spectrum, which more or less reflects the critical temperature $1/T_c \simeq 0.2$ GeV^{-1}, is nearly the same as that of the hadronic background. However, there is one difference between hadronic sources and the thermal radiation: the first is proportional to the charged multiplicity (N_{ch}), whereas the latter may have a quadratic dependence on N_{ch}. To study the multiplicity dependence of the photons, the ^{16}O and ^{32}S data set was split into two and three bins of E_T, equivalent to bins of charged multiplicity [6]. The average E_T is measured in the pseudorapidity range $-0.1 < \eta < 2.9$. The results are listed in Table 3 and plotted in Fig. 5 together with the p+W data and the high-momentum bin. The full line in Fig. 5 represents the expected value for hadronic sources, the dashed line the uncertainty on this expectation, as discussed above. The small difference for p-W and O(S)+W is due to differences in the $p_\perp$ spectra of π^0's. For the S+W(Pt) data, there is a slight tendency of r_γ to increase with E_T, but within the statistical errors no conclusion can be drawn from this, even more since the average absolute value does agree very well with the expectation.

8. Conclusion

The $p_\perp$ spectra of photons were measured for p+W, ^{16}O+W and ^{32}S+W(Pt) at 200 GeV/u. Within the statistical (4% - 11%) and systematic errors (9%), these spectra agree in shape and absolute cross section with the expected photon spectra

from hadronic sources, which has also uncertainties of about 9%, mainly due to lack of knowledge about η production.

To measure the predicted rate $r_{\gamma,thermal}$ of $\lesssim 5\%$ in the range $0.1 < p_\perp < 2.5$ [3], a sensitivity of about $\simeq 1\%$ for direct photons compared to the hadronic background is needed to measure conclusively thermal photons radiated from a hot state formed in pA or AA collisions.

We are grateful to the CERN Accelerator Division for the excellent performance of the machine complex, and would like to thank the staff of the GSI computer centre for the resources and invaluable help in the analysis of the data. We thank CERN and the Institutes collaborating in HELIOS for their contributions. The support given by the Natural Sciences and Engineering Research Council of Canada, the Institut de Recherche Fondamentale (CEA, France), the German Federal Minister for Research and Technology, the Instituto Nazionale di Fisica Nucleare of Italy, the Science Research Council of Sweden, the Science and Engineering Research Council of United Kingdom, the U.S. Department of Energy and the U.S.-Israel Bi-National Science Foundation is gratefully acknowledged.

References

1. See, for example, Proc. of the Quark Matter Conferences in Brookhaven (1984), Helsinki (1984) and Asilomar (1986)

   M. Gyulassy, Nucl. Phys. **A418** (1984) 59c.

2. E. L. Feinberg, Nuovo Cimento **A34** (1976) 391.

   L. D. McLerran, T. Toimela, Phys. Rev. **D31** (1985) 545.

   K. Kajantie, H. I. Miettinen, Z. Phys. **C9** (1981) 341.

   E. V. Shuryak, Sov. J. Nucl. Phys. **28(3)** (1978) 408.

3. M. Neubert, Z. Phys. **C42** (1989) 231.

4. J. D. Bjorken, L. McLerran, Phys. Rev. **D31** (1985) 63.

5. J. Schukraft, Z. Phys. **C38** (1988) 59.

6. T. Åkesson, et al., to be published in Z. Phys. C.

7. H.W. Bartels, PHD thesis, University of Heidelberg, (1989).

8. A. Chilingarov et al., Nucl. Phys. **B151** (1979) 29.

   R. Singer et al., Phys. Lett. **B60** (1976) 385.

   C. Kourkoumelis et al., Phys. Lett. **B84** (1979) 277.

   M.G. Albrow et al., Nucl. Phys. **B155** (1979) 39.

   M. Diakonou et al., Phys. Lett. **B89** (1980) 432.

   P. Perez et al., Phys. Lett. **B112** (1982) 260.

   M. Basile et al., Nuovo Cimento **A65** (1981) 421.

   T. Åkesson et al., Z. Phys. **C18** (1983) 5.

   T. Åkesson et al., Phys. Lett. **B178** (1986) 447.

9. M. Bourquin and J. M. Gaillard, Nucl. Phys. **B114** (1976) 334.

10. T. Åkesson, et al., Z. Phys. **C38** (1988) 383.

    T. Åkesson, et al., to be published in Z. Phys. C.

11. HELIOS Collaboration, publication in preparation.

12. L. Dragon, WA80-Collaboration, private communication

13. B. Alper et al., Nucl. Phys. **B100** (1975) 237.

Figure captions

Fig. 1 Schematic top view of the External Spectrometer in HELIOS with a photon produced at the target and measured in the External Spectrometer

Fig. 2 Relative energy distribution of the electrons: $\epsilon \equiv E_{e^-}/E_\gamma$-distribution for ideal detector, real data, MC data (normalized at $\epsilon = 0.5$), and photon background (like-sign pairs)

Fig. 3 $p_\perp$ spectra of photons for
a) p+W at 200 GeV ($E_T > 20$ GeV in $-0.1 < \eta < 2.9$)
b) ^{16}O+W at 200 GeV/u ($E_T > 60$ GeV in $-0.1 < \eta < 2.9$)
c) ^{32}S+W at 200 GeV ($E_T > 80$ GeV in $-0.1 < \eta < 2.9$)
The errors shown are statistical; the systematic errors are estimated to be about 9%.

Fig. 4 Ratios of the $p_\perp$ spectra of Figs. 3b and 3a (a) and Figs. 3c and 3a (b), normalized to the integrals. The errors shown are statistical; the systematic errors are estimated to be about 9%.

Fig. 5 $r_\gamma \equiv \gamma_{all}/\pi^0$ measured over the integrated range $p_\perp > 100$ MeV/c and $p_\perp > 600$ MeV/c vs. $\langle E_T \rangle$ in $-0.1 < \eta < 2.9$. The smaller error bars always show the statistical error, the larger ones the quadratic sum of statistical and systematic uncertainty. The full line represents the expected values r_{γ,h^0} from hadronic decays, the dotted line the uncertainties of this expectation.

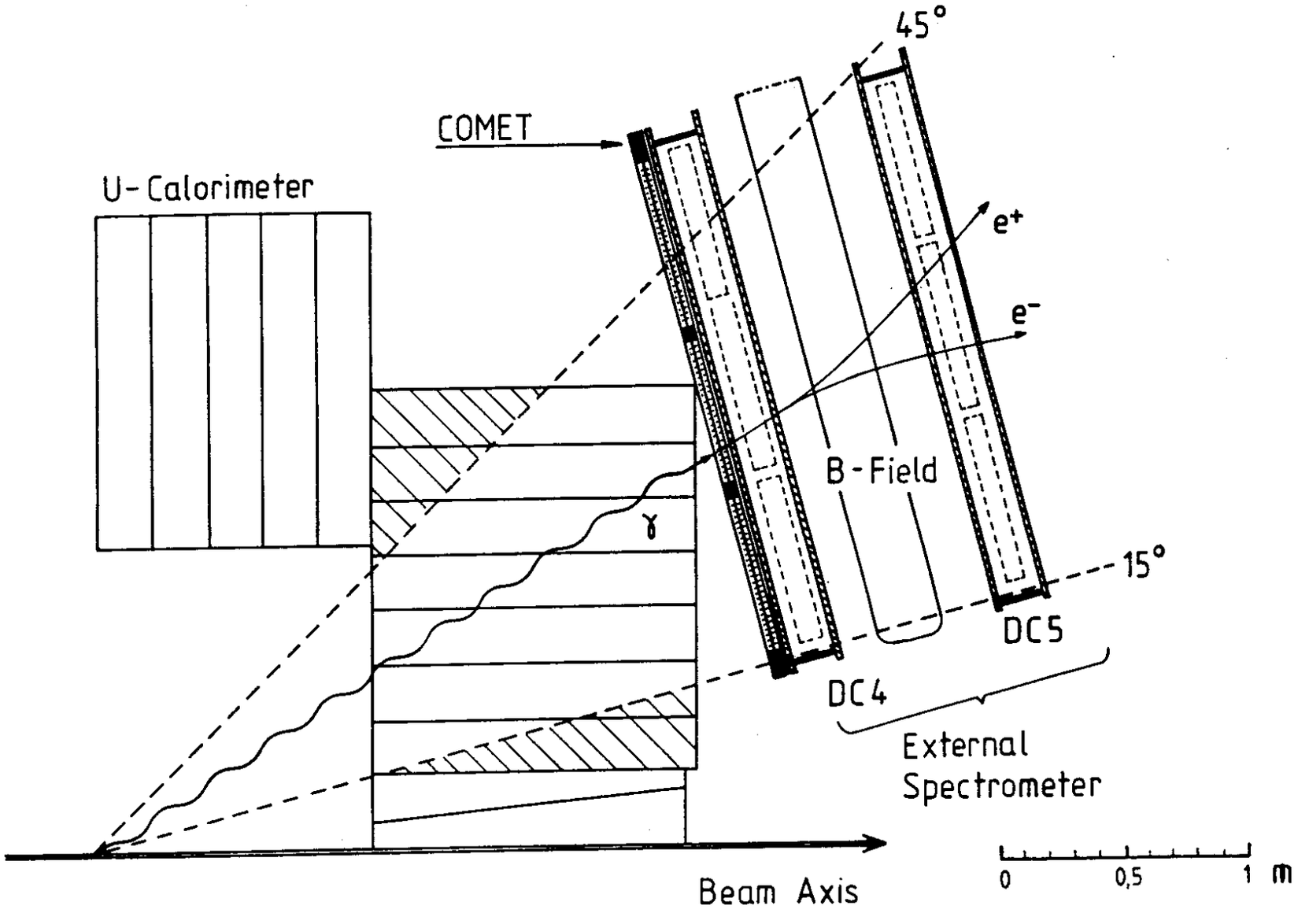
45°
COMET
U-Calorimeter
e+
e-
B-Field
γ
15°
DC5
DC4
External
Spectrometer
Beam Axis
0
0,5
1 m

Fig. 1

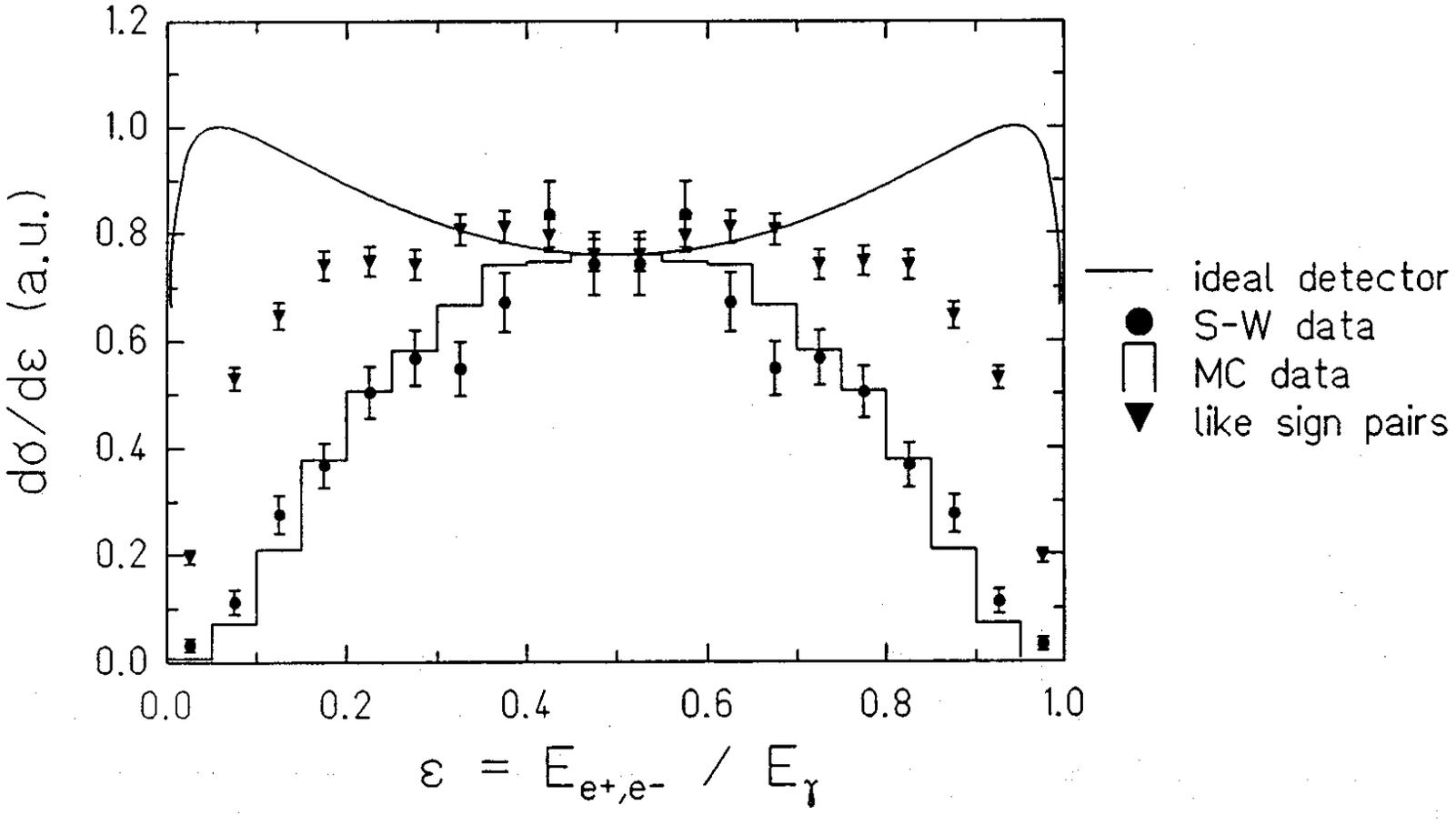
1.2
1.0
0.8
0.6
0.4
0.2
0.0
dσ/dε (a.u.)
0.0
0.2
0.4
0.6
0.8
1.0
ε = E e+,e- / E γ
ideal detector
S-W data
MC data
like sign pairs

Fig. 2

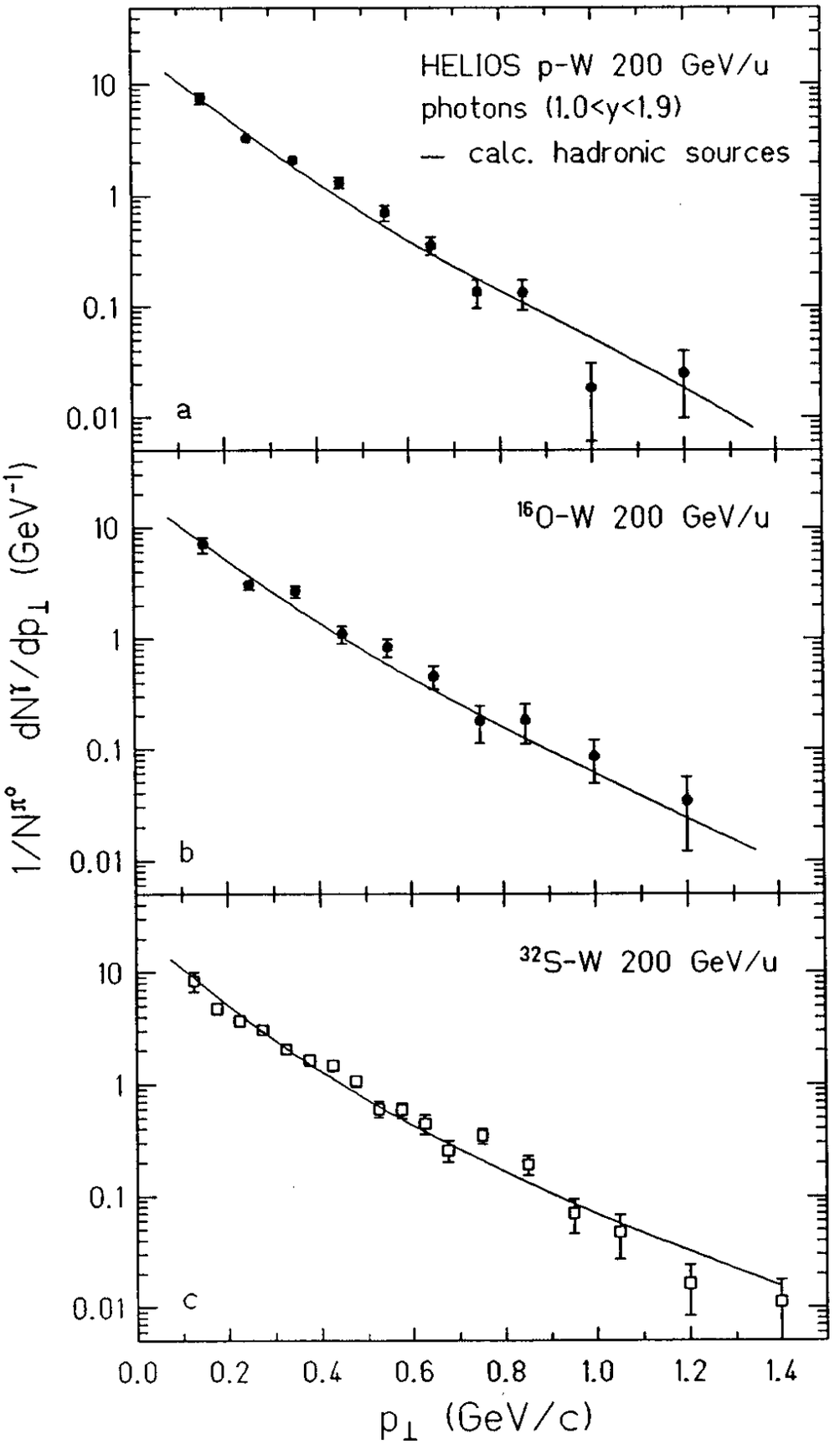
HELIOS p-W 200 GeV/u
photons (1.0<y<1.9)
— calc. hadronic sources
a
^{16}O-W 200 GeV/u
b
^{32}S-W 200 GeV/u
c
$1/N^{\pi^0}\ dN^{\gamma}/dp_{\perp}\ (GeV^{-1})$
$p_{\perp}$ (GeV/c)
10
1
0.1
0.01
0.0
0.2
0.4
0.6
0.8
1.0
1.2
1.4

Fig. 3

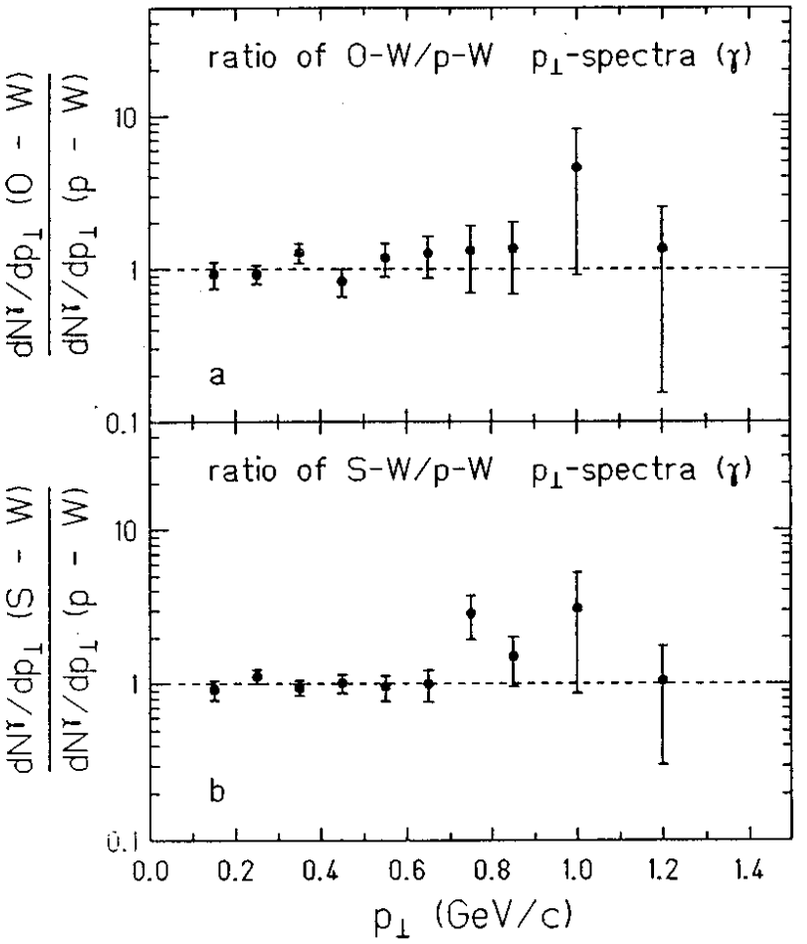
ratio of O-W/p-W $p_\perp$-spectra (γ)
$\frac{dN_\gamma/dp_\perp\ (O-W)}{dN_\gamma/dp_\perp\ (p-W)}$
a
ratio of S-W/p-W $p_\perp$-spectra (γ)
$\frac{dN_\gamma/dp_\perp\ (S-W)}{dN_\gamma/dp_\perp\ (p-W)}$
b
10
1
0.1
0.0
0.2
0.4
0.6
0.8
1.0
1.2
1.4
$p_\perp$ (GeV/c)

Fig. 4

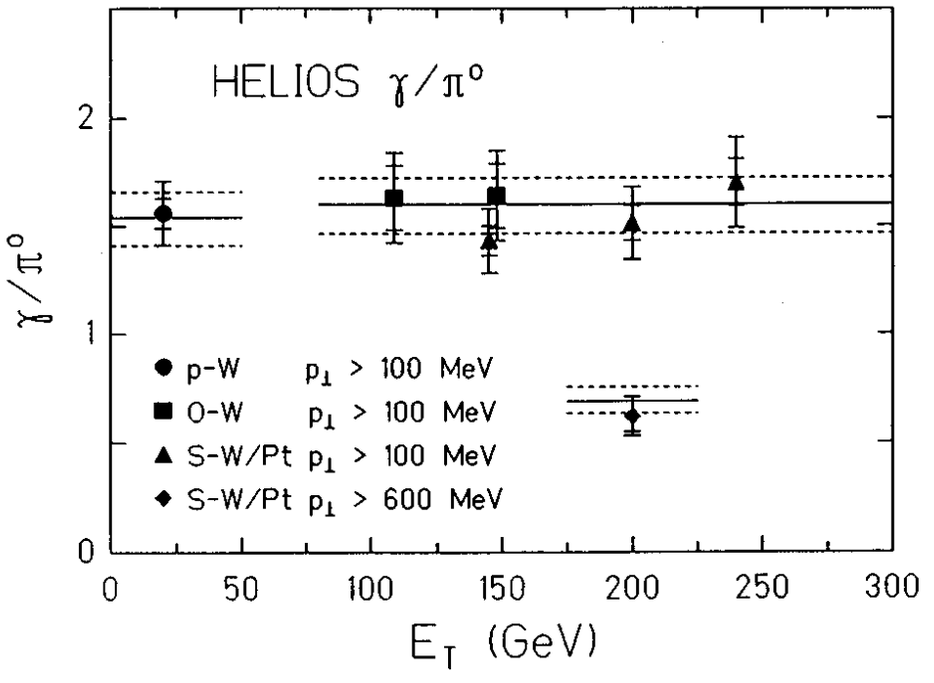
HELIOS γ/π^0
γ/π^0
p-W $p_\perp$ > 100 MeV
O-W $p_\perp$ > 100 MeV
S-W/Pt $p_\perp$ > 100 MeV
S-W/Pt $p_\perp$ > 600 MeV
2
1
0
0
50
100
150
200
250
300
E_T (GeV)

Fig. 5